Simultaneous measurement of core electron temperature and density fluctuations during electron cyclotron heating on DIII-D

Citation: White, A. E. et al. "Simultaneous measurement of core electron temperature and density fluctuations during electron cyclotron heating on DIII-D." Physics of Plasmas 17 (2010): 020701. © 2010 American Institute of Physics

As Published: http://dx.doi.org/10.1063/1.3318469

Publisher: American Institute of Physics

Persistent URL: http://hdl.handle.net/1721.1/66225

Version: Final published version: final published article, as it appeared in a journal, conference proceedings, or other formally published context

Simultaneous measurement of core electron temperature and density fluctuations during electron cyclotron heating on DIII-D

A. E. White,[1,a] L. Schmitz,[1] W. A. Peebles,[1] T. L. Rhodes,[1] T. A. Carter,[1] G. R. McKee,[2] M. W. Shafer,[2] G. M. Staebler,[3] K. H. Burrell,[3] J. C. DeBoo,[3] and R. Prater[3]
[1]*Department of Physics and Astronomy, University of California-Los Angeles, Los Angeles, California 90095, USA*
[2]*Department of Engineering, University of Wisconsin, Madison, Wisconsin 53706, USA*
[3]*General Atomics, San Diego, California 92186, USA*

(Received 14 October 2009; accepted 25 January 2010; published online 18 February 2010)

New measurements show that long-wavelength ($k_\theta \rho_s < 0.5$) electron temperature fluctuations can play an important role in determining electron thermal transport in low-confinement mode (L-mode) tokamak plasmas. In neutral beam-heated L-mode tokamak plasmas, electron thermal transport and the amplitude of long-wavelength electron temperature fluctuations both increase in cases where local electron cyclotron heating (ECH) is used to modify the plasma profiles. In contrast, the amplitude of simultaneously measured long-wavelength density fluctuations does not significantly increase. Linear stability analysis indicates that the ratio of the trapped electron mode (TEM) to ion temperature gradient (ITG) mode growth rates increases in the cases with ECH. The increased importance of the TEM drive relative to the ITG mode drive in the cases with ECH may be associated with the increases in electron thermal transport and electron temperature fluctuations.
 [doi:10.1063/1.3318469]

The importance of long-wavelength turbulent fluctuations in determining electron thermal transport in the core of tokamak plasmas is of considerable interest to the field of magnetically confined fusion. In the absence of magnetohydrodynamic (MHD) instabilities, small amplitude ($\sim 1\%$), low frequency ($\omega < \Omega_{ci}$, where Ω_{ci} is the ion cyclotron frequency) turbulent fluctuations associated with drift-wave-type instabilities are widely believed to drive radial transport.[1] The turbulence driven transport can lead to heat and particle losses that reduce the performance of magnetically confined fusion devices.[2] One expectation from drift-wave theory that can be tested directly is that the ratio of electron temperature and density fluctuation amplitudes, $(\tilde{T}_e/T_e)/(\tilde{n}/n)$, should scale with the ratio of linear growth rates of the trapped electron mode (TEM) and the ion temperature gradient (ITG) mode, $\gamma_{\mathrm{TEM}}/\gamma_{\mathrm{ITG}}$.[3,4] To test this, multifield fluctuation measurements are needed. Electron temperature fluctuations and density fluctuations have previously been studied in tokamak experiments[5–7] during electron cyclotron heating (ECH), but the two fluctuating fields were not measured simultaneously. We present here the first simultaneous measurements of long-wavelength electron temperature fluctuations and density fluctuations in the core of an L-mode tokamak plasma heated with neutral beams and ECH.

The experiment was performed on the DIII-D tokamak (major radius $R=1.67$ m, minor radius $a=0.61$ m).[8] The discharges have magnetic field $B_T \approx 2.0$ T, plasma current $I_p=1$ MA, with edge safety factor $q_{95} \approx 5.2$ in the time period of interest, and are inner wall limited. A first discharge is heated with 2.5 MW of neutral beam power injected in the direction of the plasma current beginning early in time $t=300$ ms. The L-mode plasma of interest ($1500 < t < 1800$ ms) is sawtooth-free and MHD-free. In a second discharge, in addition to 2.5 MW of beam power, 2.5 MW of ECH power (110 GHz, X-mode) is deposited at the second harmonic electron cyclotron emission (ECE) resonance layer at $\rho=0.17$ beginning at $t=1400$ ms. The radial profiles of electron (T_e) and ion temperature (T_i) and density (n_e) with (red) and without (black) ECH are shown in Fig. 1 and are plotted versus ρ, the normalized square root of the toroidal flux. Derivatives are calculated with respect to ρ', the square root of the toroidal flux (not normalized). Radial locations of interest for turbulence measurements, local gradient values, and linear stability calculations are referenced in values of ρ. The profiles shown in Fig. 1 represent the average from an ensemble of 100 spline fits to the data at $t=1605$ ms. The data are randomly varied within the measurement error before each spline fit using a Monte Carlo method. Dotted lines indicate one sigma error bar from the resulting distribution of 100 fits, representing an estimate of random experimental error in the profiles. With ECH, T_e increases a factor of 2 on axis and a factor of 1.5 at the fluctuation measurement locations $\rho=0.5$, 0.6, and 0.7. The density profile is matched in the two discharges using feedback control and edge gas puff fueling; T_i increases 20%–30% in the region of interest. The electron temperature gradient ∇T_e increases 50%, with little to no change in the ion temperature gradient ∇T_i or the density gradient ∇n. The normalized gradient scale length is defined for temperature, for example, as $a/L_T = a/|(T/(dT/d\rho'))|$, where a is the plasma minor radius at the last closed flux surface at the midplane. During ECH, in the fluctuation measurement region, $0.5 < \rho < 0.7$, there is a de-

[a]Present address: Department of Nuclear Science and Engineering, Massachusetts Institute of Technology, Cambridge, Massachusetts 02139, USA. Electronic mail: whitea@mit.edu.

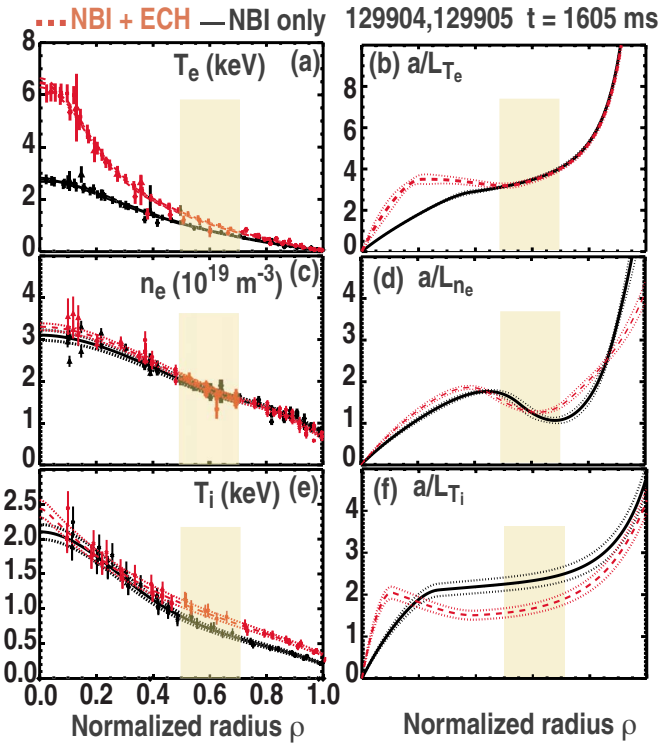

FIG. 1. (Color online) Radial profiles of (a) electron temperature and (b) a/L_{T_e}, (c) density, and (d) a/L_{n_e}, (e) ion temperature and (f) a/L_{T_i} for the cases with ECH and NBI heating (red dashed) and NBI heating only (black solid) are plotted vs ρ, the normalized square root of the toroidal flux. Derivatives are calculated with respect to non-normalized square root of toroidal flux. The dotted lines indicate the standard deviation calculated from an ensemble of 100 profile fits. ECH power is deposited at $\rho \sim 0.17$ in the case with ECH (red). Electron temperature and density fluctuations are measured at $\rho=0.5$, 0.6, and 0.7 (shading).

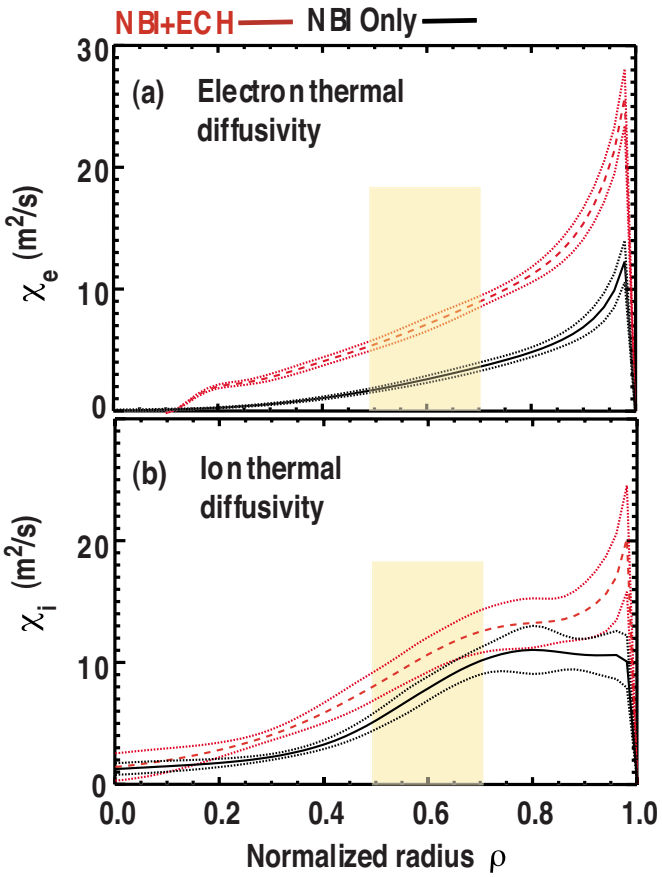

FIG. 2. (Color online) (a) χ_e and (b) χ_i in cases with no ECH (black solid) and with ECH (red dashed). The mean diffusivity and standard deviation (dotted lines) are calculated from an ensemble of 100 ONETWO analyses using as input 100 sets of spline fits to measured radial profiles. Electron temperature and density fluctuations are measured between $0.5<\rho<0.7$ (yellow shading).

crease in a/L_{T_i} due mainly to increases in T_i, a/L_n increases, and a/L_{T_e} does not change outside the error bars. Effective charge state Z_{eff} has increased from 1.7 to 2.2. Overall, the increases in T_e/T_i and L_{T_i}/L_{T_e} and decrease in collisionality $\nu_{\text{eff}}=\nu_{ei}/\omega_{\text{de}}$ (Ref. 9) by a factor of 2 are expected to increase the TEM drive relative to ITG mode drive according to drift-wave theory. The ECH also leads to changes in the radial electric field profile, but there is no change in the $E\times B$ shearing rate outside error bars.

To evaluate the changes in transport between the two cases, time-independent power balance analysis is performed with the ONETWO code.[10] The 100 fits to measured profiles (T_e, T_i, n_e, toroidal rotation, and impurity density) are used as input to the radial power balance analyses. In Fig. 2 the mean electron (χ_e) and ion (χ_i) thermal diffusivities and standard deviations are calculated from the resulting ensemble of 100 ONETWO analyses. Figure 2(a) shows that the experimentally inferred electron thermal diffusivity χ_e increases factors of 2.5–3.5 during ECH. The ion thermal diffusivity χ_i, Fig. 2(b), tends to increase as well, but changes are just outside error bars in the region of interest, $0.5<\rho<0.7$.

To monitor changes in core turbulence, long wavelength fluctuations ($k_\theta \rho_s < 0.5$) are measured at three radial locations: $\rho=0.5$, 0.6, and 0.7 with the beam emission spectroscopy (BES) system[11] and the correlation electron cyclotron emission (CECE) diagnostic.[12] Here k_θ is the wavenumber of the fluctuations, θ is poloidal direction, and ρ_s is the ion sound gyroradius. BES and CECE are sensitive to local, long-wavelength density fluctuations $\tilde{n}/n$ and electron temperature fluctuations $\tilde{T}_e/T_e$, respectively. The changes in the fluctuation spectra at $\rho \approx 0.7$ during ECH are shown in Fig. 3.

The fluctuation data are averaged over 200 ms between $t=1500$ and 1700 ms to improve the signal to noise ratio. At $\rho=0.7$, the measured electron temperature fluctuation level (obtained by integrating the cross-power spectrum between 40 and 400 kHz) increases by 50% from $\tilde{T}_e/T_e=1.0\pm0.2\%$ in the beam-only plasma to $\tilde{T}_e/T_e=1.5\pm0.2\%$ in the plasma with additional ECH, Fig. 3(b). In contrast, density fluctuation level (40–400 kHz) does not change outside the experimental uncertainty, $\tilde{n}/n \approx 1.2\pm0.18\%$ in both cases, Fig. 3(a). The frequency range of 40–400 kHz is chosen to avoid low-frequency noise contributions in the BES data arising from the neutral beam. Radial profiles of $\tilde{T}_e/T_e$ and $\tilde{n}/n$ are shown in Fig. 4. The density fluctuation amplitudes, Fig. 4(a), do not increase with ECH at any measurement location. In contrast, the electron temperature fluctuation amplitudes, Fig. 4(b), increase at all radial locations, with the largest increase at $\rho=0.5$, where $\tilde{T}_e/T_e$ increases at least a factor of

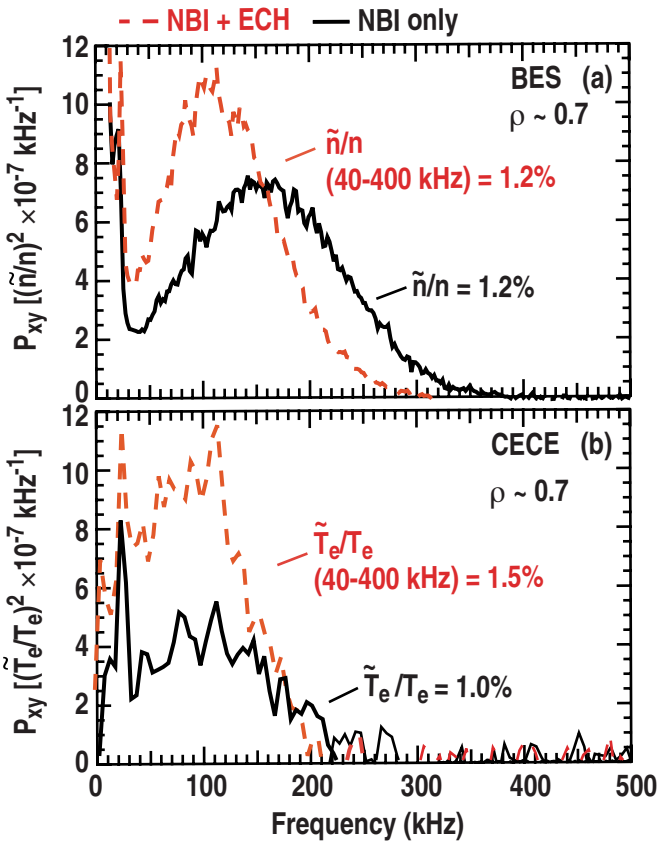

FIG. 3. (Color online) Spectra of (a) density fluctuations and (b) electron temperature fluctuations measured at $\rho \sim 0.7$ in the L-mode with ECH and NBI heating (red dashed) and with NBI heating only (black solid). Fluctuation levels (40–400 kHz) are recorded in the figure. Electron temperature fluctuation amplitude increases 50% in the case with ECH; density fluctuation amplitude does not change.

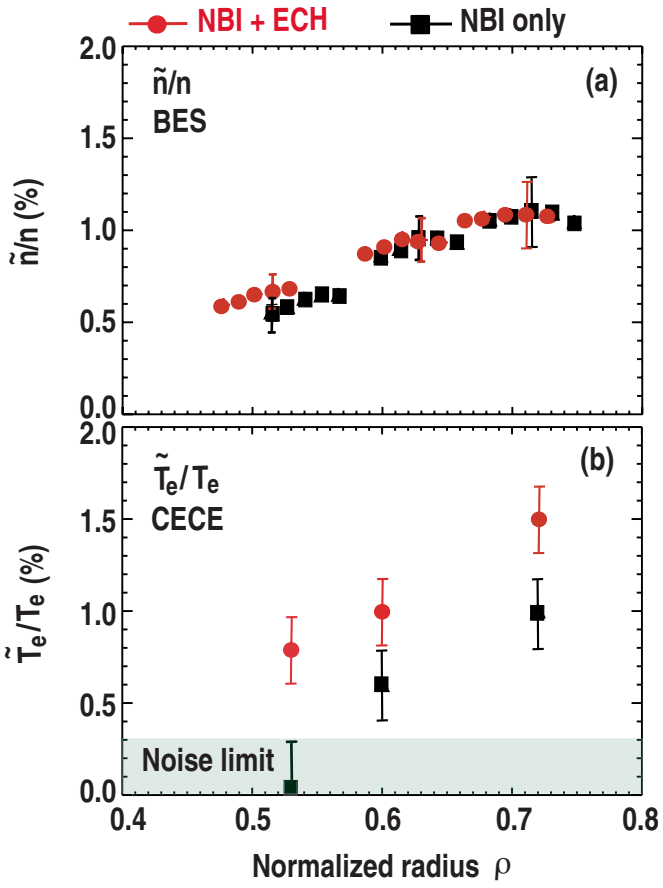

FIG. 4. (Color online) The profile of the relative amplitudes of (a) density fluctuations and (b) electron temperature fluctuations with ECH and NBI heating (red circles) and with NBI heating only (black squares). The green shaded region in (b) indicates the noise limit for $\tilde{T}_e/T_e$ measurements.

2.5 from below the noise level. The spectral narrowing and downshifts observed in the density fluctuation spectrum correspond to a reduction in $E\times B$ velocity during ECH. Changes in the spectral shape for the temperature fluctuations with ECH are less obvious, as an increase in $\tilde{T}_e/T_e$ at many frequencies could mask typically observed Doppler shifts.[12]

The increase in the ratio $(\tilde{T}_e/T_e)/(\tilde{n}/n)$ may be due to increases in the ratio of the linear mode growth rates $\gamma_{\mathrm{TEM}}/\gamma_{\mathrm{ITG}}$,[3,4] as $\tilde{T}_e/T_e$ may be more sensitive to changes in the TEM drive. A connection between electron temperature fluctuations and the TEM has been suggested previously[13] and would be consistent with the nature of X-mode radiometer measurements of temperature fluctuations.[5] Linear stability analysis for the beam-heated L-mode plasmas with and without ECH is performed with the trapped gyro-Landau fluid (TGLF) moment equations.[14] The analysis takes experimental profiles as input and calculates the linear growth rates γ_{lin} and real frequencies f_{lin} of the electron mode ($\gamma_{\mathrm{elec}}, f_{\mathrm{lin}} > 0$) and ion mode ($\gamma_{\mathrm{ion}}, f_{\mathrm{lin}} < 0$). Here we associate the long wavelength electron branch with the TEM, the ion branch with the ITG mode. The wavenumber spectra of the linear growth rates γ_{TEM} and γ_{ITG} are shown in Fig. 5. The same 100 fits to the measured profiles used for power balance analysis are used as input to the TGLF analysis. In Fig. 5 the mean growth rates and standard deviations are calculated from the resulting ensemble of 100 TGLF analyses. In the case with ECH, γ_{TEM} has increased and γ_{ITG} has decreased at all three radii in the long wavelength range of interest $k_\theta \rho_s < 0.8$. The changes are outside the one sigma error bars, which represent the uncertainty of the calculated growth rates due to random error in the input profiles. Note that changes in γ_{ITG} and γ_{TEM} occur in the wavenumber range where the CECE and BES fluctuation diagnostics are expected to be most sensitive (yellow shading) and also outside this range. Numerical gyrokinetic simulations have shown that nonlinear effects of fully developed turbulence tend to produce maximum transport at lower wavenumbers than where the peak in linear growth rate occurs.[15] The experimental $E\times B$ shearing rate in these plasmas is calculated from the radial electric field profile, which is determined using charge exchange recombination spectroscopy[16] measurements of the poloidal and toroidal impurity carbon rotation velocities. There is no difference outside the error bars in the $E\times B$ shearing rate for the two experimental cases of interest, so we compare the average $E\times B$ shearing rate from the two cases with the linear growth rates. Where the $E\times B$ shearing rate exceeds the linear mode growth rate it can lead to stabilization of the mode.[17] By comparing the elongation corrected, flux surface averaged Waltz–Miller $E\times B$ shearing

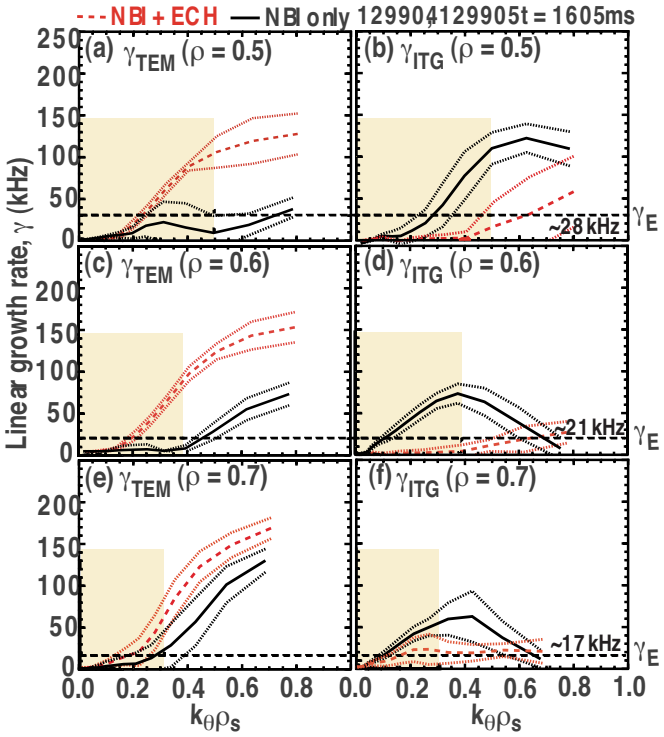

FIG. 5. (Color online) The change in [(a), (c), and (e)] TEM and [(b), (d), and (f)] ITG mode growth rates at three radii of interest is shown. The horizontal dashed line indicates the two-shot average (with and without ECH) of the flux-surface averaged $E\times B$ shearing rate. The estimated wavenumber sensitivity range for the fluctuation diagnostics is indicated with shading.

rate[18] with the linear growth rates, we find that shear suppression may be important at long wavelengths.

In conclusion, new multifield fluctuation measurements at DIII-D show that long-wavelength electron temperature fluctuations can play an important role in determining electron thermal transport in L-mode tokamak plasmas. In this experiment, χ_e and the amplitude of long-wavelength electron temperature fluctuations both increase in beam-heated L-mode plasmas where local ECH is used to modify the plasma profiles. In contrast, the amplitude of long-wavelength density fluctuations does not change. Linear stability analysis indicates that the linear growth rate ratio $\gamma_{\mathrm{TEM}}/\gamma_{\mathrm{ITG}}$ at long wavelengths ($k_\theta\rho_s<0.8$) increases when the experimental ratio of fluctuation levels $(\tilde{T}_e/T_e)/(\tilde{n}/n)$ increases, which is consistent with expectations from drift-wave theory. The trend that $\gamma_{\mathrm{TEM}}/\gamma_{\mathrm{ITG}}$ increases during ECH indicates that the TEM is playing a larger role in governing electron heat transport in those cases, which may be the reason for the observed increases in χ_e and $\tilde{T}_e/T_e$ in those cases. However, nonlinear turbulence simulations are needed to fully explore the details of changes in the turbulence drive and the effects of $E\times B$ shear. These new multifield fluctuation measurements may help explain past experimental results where transport changed significantly although long-wavelength density fluctuation amplitudes did not change.[7,19]

This work was supported in part by the U.S. Department of Energy under Contract Nos. DE-AC05-06IR23100, DE-FG03-01ER54615, DE-FG02-89ER53296, and DE-FC02-04ER54698. A.E.W. thanks M. E. Austin for ECE analysis, C. C. Petty for error analysis discussions, R. J. Groebner for CER analysis, M. A. Makowski for MSE and EFIT analysis, and the entire DIII-D team for their support of these experiments.

[1] W. Horton, Rev. Mod. Phys. **71**, 735 (1999).
[2] J. Wesson, *Tokamaks*, 3rd ed. (Oxford University Press, New York, 2004).
[3] H. T. Evensen, R. J. Fonck, S. F. Paul, G. Rewoldt, S. D. Scott, W. M. Tang, and M. C. Zarnstorff, Nucl. Fusion **38**, 237 (1998).
[4] J. Dannert and F. Jenko, Phys. Plasmas **12**, 072309 (2005).
[5] H. J. Hartfuß, M. Häse, C. Watts, M. Hirsch, T. Geist, and the W7-AS Team, Plasma Phys. Controlled Fusion **38**, A227 (1996).
[6] C. Watts, Fusion Sci. Technol. **52**, 176 (2007).
[7] T. L. Rhodes, W. A. Peebles, M. A. Van Zeeland, J. S. deGrassie, R. V. Bravenec, K. H. Burrell, J. C. DeBoo, J. Lohr, C. C. Petty, X. V. Nguyen, E. J. Doyle, C. M. Greenfield, L. Zeng, and G. Wang, Phys. Plasmas **14**, 056117 (2007).
[8] J. L. Luxon, Nucl. Fusion **42**, 614 (2002).
[9] F. Ryter, C. Angioni, A. G. Peeters, F. Leuterer, H.-U. Fahrbach, and W. Suttrop, Phys. Rev. Lett. **95**, 085001 (2005).
[10] H. E. St John, T. S. Taylor, Y. R. Lin-Liu, and A. D. Turnbull, Plasma Phys. Controlled Nucl. Fusion Res. **3**, 603 (1994).
[11] G. R. McKee, R. Ashley, R. Durst, R. Fonck, M. Jakubowski, K. Tritz, K. Burrell, C. Greenfield, and J. Robinson, Rev. Sci. Instrum. **70**, 913 (1999).
[12] A. E. White, L. Schmitz, G. R. McKee, C. Holland, W. A. Peebles, T. A. Carter, M. W. Shafer, M. E. Austin, K. H. Burrell, J. Candy, J. C. DeBoo, E. J. Doyle, M. A. Makowski, R. Prater, T. L. Rhodes, G. M. Staebler, G. R. Tynan, R. E. Waltz, and G. Wang, Phys. Plasmas **15**, 056116 (2008).
[13] C. E. Thomas and R. F. Gandy, Rev. Sci. Instrum. **61**, 3570 (1990).
[14] G. M. Staebler, J. E. Kinsey, and R. E. Waltz, Phys. Plasmas **14**, 055909 (2007).
[15] R. E. Waltz, J. Candy, and M. Fahey, Phys. Plasmas **14**, 056116 (2007).
[16] W. M. Solomon, K. H. Burrell, P. Gohil, R. J. Groebner, and L. R. Baylor, Rev. Sci. Instrum. **75**, 3481 (2004).
[17] K. H. Burrell, Phys. Plasmas **4**, 1499 (1997).
[18] J. E. Kinsey, R. E. Waltz, and J. Candy, Phys. Plasmas **14**, 102306 (2007).
[19] G. R. McKee, R. Fonck, D. Gupta, D. Schlossberg, M. Shafer, R. Groebner, C. Petty, M. Murakami, W. Horton, T. Rhodes, G. Wang, L. Zeng, D. Rudakov, J. Boedo, and J. Kinsey, Bull. Am. Phys. Soc. **48**, 259 (2003).